Bromate incorporation in calcite and aragonite

Available online at www.sciencedirect.com

ScienceDirect

Geochimica et Cosmochimica Acta 324 (2022) 17–25

Geochimica et Cosmochimica Acta

www.elsevier.com/locate/gca

Bromate incorporation in calcite and aragonite

Scott D. Midgley [a], Dominik Fleitmann [b,c], Ricardo Grau-Crespo [a,*]

[a] Department of Chemistry, University of Reading, Reading RG6 6DX, United Kingdom
[b] Department of Archaeology, University of Reading, Reading RG6 6AB, United Kingdom
[c] Department of Environmental Sciences, University of Basel, Basel CH-4056, Switzerland

Received 27 June 2021; accepted in revised form 24 February 2022; available online 2 March 2022

Abstract

The presence of bromine as a trace-element in calcium carbonate speleothems constitutes a useful proxy of past volcanic activity, thus helping to provide input parameters for climate model simulations and risk assessment. However, the chemical nature of bromine-containing impurities in the calcium carbonate phases forming speleothems is not understood, which limits interpretation of experimental measurements on speleothems. We present here a computer simulation study, based on quantum mechanical calculations, of the incorporation of bromine as BrO_3^- oxyanions in $CaCO_3$ polymorphs calcite and aragonite. We discuss how the relative distributions of bromate oxyanions and charge-compensating alkali-metal cations are determined by the interplay between an impurity binding effect (which is stronger for aragonite than for calcite, and changes in the order Li < Na < K) and a configurational entropic effect that tends to disassociate the impurities. For concentrations above parts-per-million, bromate impurities can be expected to be paired, in nearest-neighbour configurations, with the compensating cations. Bromate substitution, compensated by sodium or potassium cations, is predicted to be metastable with respect to phase separation of the impurities as solid $NaBrO_3$ or $KBrO_3$ phases, respectively, but the solubility limits of BrO_3^- in calcite and aragonite are still higher than those calculated for tetrahedral oxyanions $(SO_4)^{2-}$ and $(MoO_4)^{2-}$ that are used as alternative volcanic records in speleothems.

Keywords: Calcium carbonate; Calcite; Aragonite; Bromate

1. INTRODUCTION

Volcanic eruptions impact local and global climates (Robock, 2000; Zielinski, 2000; Sigl et al., 2013). They have been shown to significantly disrupt transfer of solar radiation, leading to a cooling effect that can affect large areas of the planet for several years and possibly even for decades (Minnis et al., 1993; Robock and Free, 1995). Recent research efforts have attempted to build accurate reconstructions of volcanic activity spanning millennia, to understand the historical impact of these significant geological events on global climate. Though instrumental and historical records of volcanic activity exist for a few centuries, obtaining information on volcanic eruptions further back in time requires analysis of naturally occurring archives to reveal the explosive history of volcanoes. Ice-cores (Zielinski et al., 1994; Yalcin et al., 2007; Severi et al., 2012), tree rings (McCarroll and Loader, 2004) and marine sediments (Voelker, 2002) are all well-established records of past volcanic activity, because they provide a naturally undisturbed environment in which geochemical tracers and tephra layers may be preserved over long timescales. Proxies contained within these geological archives, such as trace-element concentrations (Hartland et al., 2012) and $\delta^{18}O$ isotopic composition (Marshall et al., 2009) have been used to derive valuable information about past climate

* Corresponding author.
E-mail address: r.grau-crespo@reading.ac.uk (R. Grau-Crespo).

https://doi.org/10.1016/j.gca.2022.02.028
0016-7037/

and compositions of the atmosphere. Speleothems are another example of such an archive, which have shown increasing promise as paleovolcanic records in recent years (Finch et al., 2001; Fairchild and Treble, 2009; Badertscher et al., 2014; Ünal-İmer et al., 2015). Speleothems have two key advantages over ice-cores as archives for paleoclimate research. The first is that speleothem formation is not linked to the low temperatures associated with high latitudes. This is important as many of the most explosive volcanoes are in the tropics and subtropics and, thus, far away from the polar ice cores. The second advantage is that the uranium–thorium dating technique is well established for calcium carbonates, meaning that accurate speleothem dating is relatively straightforward (Dorale et al., 2004; St Pierre et al., 2009). Calcite is the most stable calcium carbonate phase over long geological timescales, and it comprises the majority of speleothems. Aragonite is metastable under some geochemical conditions, and forms speleothems in some rarer cases (Given and Wilkinson, 1985; Railsback et al., 1994; De Choudens-Sanchez and Gonzalez, 2009).

Major volcanic eruptions affect the chemical composition of the atmosphere and pedosphere (soil layers). Elements such as sulphur, molybdenum and bromine are known to be in high relative abundance following an eruption, and these may eventually become incorporated as impurities into the structures of speleothems. However, little is known about the chemical nature of these species in speleothem carbonate minerals. Recent computer modelling research by our group has considered the thermodynamics of sulphate and molybdate incorporation in speleothem minerals, finding that bulk lattice incorporation of these oxyanions is thermodynamically unfavourable, owing to significant elastic strain on the crystal caused by the large, tetrahedral anion geometries (Midgley et al., 2020), and that surfaces (or more accurately, the mineral–water interface) provide a more favourable environment for hosting the oxyanion impurities, especially in the presence of surface defects (Midgley et al., 2021).

Here, we extend our computational studies to the investigation of bromine incorporation in calcite and aragonite. Badertscher et al. (2014) have argued that bromine is probably the most effective speleothem-based paleovolcanic proxy among those investigated so far. Its fast leaching through soil layers made it detectable in speleothems found in the Sofular cave, within +/- 1–2 years of the Minoan eruption that occurred in Northern Turkey at around 1621 BCE (Friedrich et al., 2006). Very little is known about how bromine incorporates in calcium carbonate minerals. Elevated quantities of bromine in the form of hypobromite (BrO^-) are dumped into the local environment following a major volcanic eruption (Bobrowski et al., 2003; Theys et al., 2009; Hörmann et al., 2013). Hypobromite has been shown to play a critical role in tropospheric and stratospheric chemistry, with ozone depletion known to be a significant environmental consequence of this species if airborne. Its stability with respect to oxidation to bromate is low under most conditions (Engel and Perlmutter-Hayman, 1953; Lee and Lister, 1971). It is therefore reasonable to assume that incorporation of bromine in speleothems occurs in the form of the monovalent anion bromate, $(BrO_3)^-$, in analogy with the incorporation of iodine as iodate, $(IO_3)^-$, in calcium carbonate minerals (Podder et al., 2017; Feng and Redfern, 2018; Kerisit et al., 2018).

Bromate has a trigonal pyramidal geometry due to the presence of a lone pair, and therefore it is not an ideal fit to substitute the trigonal planar carbonate (CO_3^{2-}) anion. However, its flatter shape in comparison with that of tetrahedral oxyanions sulphate $(SO_4)^{2-}$ and molybdate $(MoO_4)^{2-}$ may allow easier lattice substitution. The chemistry of the aliovalent bromate/carbonate substitution is different from that of the isovalent molybdate/carbonate or sulphate/carbonate substitutions, and the charge compensating mechanisms can be expected to play a significant role in the thermodynamics of bromate incorporation. Kerisit et al. (2018) indeed found that, in the case of iodate substitution in calcite, there is an energetic preference for the compensating cation (H^+ or Na^+ in their study) to be near the iodate impurity. The ease of incorporation also depends on the host carbonate phase, and Feng and Redfern (2018) found that iodate can incorporate into crystalline bulk calcium carbonate with increasing difficulty in the order vaterite, calcite and aragonite, following the relative density of these phases.

In this work we use first principles simulation techniques to investigate for the first time the incorporation of bromate in calcite and aragonite (as the phases most interesting for our understanding of speleothems), and the relative distribution of bromate oxyanions and compensating cations in both phases. We will report the thermodynamic parameters describing the ease of incorporation in each case, both with respect to isolated ions and to competing phases. We will discuss the impurity distribution problem in terms of two thermodynamic driving forces: the binding energy between the two oppositely charged impurity defects that tends to keep the impurities paired, and the configurational entropy effects that favour unpaired impurities at low concentrations. We will also discuss the geochemical implications of our findings.

2. COMPUTATIONAL METHODS

Computer simulations within the density functional theory (DFT) were performed using the VASP code (Kresse and Furthmüller, 1996a, b), under the generalized gradient approximation (GGA) in the form of the PBE exchange–correlation functional (Perdew et al., 1996). The projector augmented wave (PAW) method (Blöchl, 1994; Kresse and Joubert, 1999) was used to describe the interaction between valence electrons and the core. The number of plane waves used in the basis was determined by a kinetic energy cutoff of 520 eV, which is 30% above the recommended value for the set of PAW potentials used, to minimise Pulay stress errors.

Calcite has a trigonal crystal system and a space group of R-3c (No. 167) (Markgraf and Reeder, 1985), and was modelled here using a hexagonal 3 × 3 × 1 supercell (54 formula units of $CaCO_3$) as shown in Fig. 1a. Aragonite is orthorhombic with the space group Pmcn (No. 62)

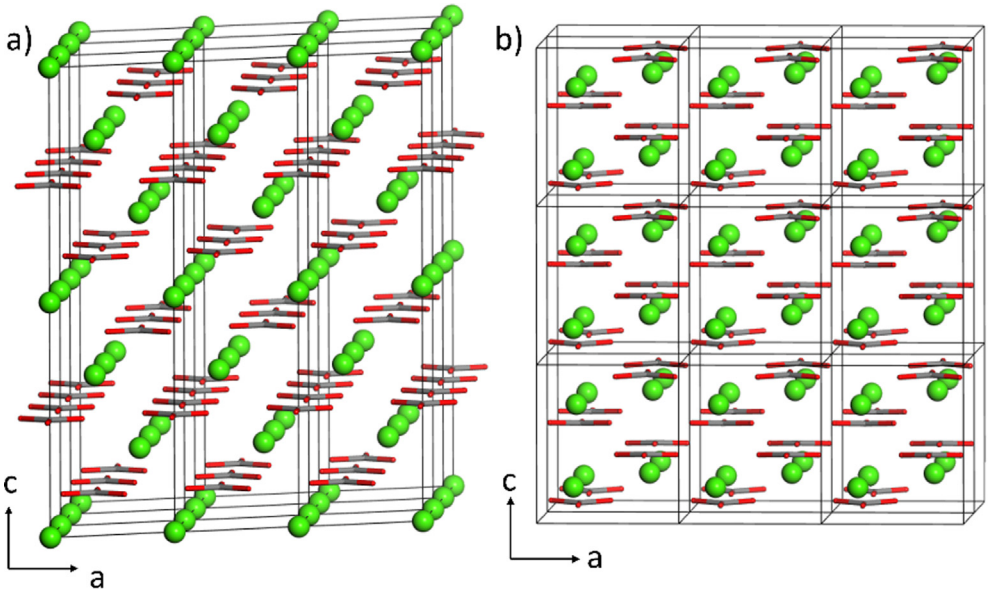

Fig. 1. Supercells of a) calcite (3 × 3 × 1) and b) aragonite (3 × 2 × 3) employed in this work. Colour code: Ca = green; C = grey; O = red.

(De Villiers, 1971), and was modelled using a 3 × 2 × 3 supercell (72 formula units; Fig. 1b). The use of relatively large supercells is needed to maximise the distance between each impurity and its periodic images (at least ~ 15 Å apart), as well as to explore the configurational space of relative positions of cation and anion impurities. The symmetrically inequivalent substitution configurations were obtained using the methodology implemented in the Site Occupancy Disorder program (SOD) (Grau-Crespo et al., 2007), which has been useful before in the investigation of impurity distribution in carbonate minerals (Ruiz-Hernandez et al., 2010; Wang et al., 2011; González-López et al., 2014). Two configurations are equivalent if they are related by a symmetry operator of the parent (unsubstituted) crystal structure. Each configuration was optimised to full geometry relaxation in VASP, and the final energies were used for statistical analysis of the impurity distribution.

The SOD/VASP analysis elucidated the minimum energy configuration of $M\mathrm{BrO_3}$ in calcite and aragonite, which was always the proximal ion-pair configuration. To calculate the energy of $\mathrm{CaCO_3}/M\mathrm{BrO_3}$ substitution in calcite, we computed two sets of energy values. The first we call the ion exchange energy E_{exch}, and is the energy of exchanging $\mathrm{Ca^{2+}}$ and $\mathrm{CO_3^{2-}}$ ions from the bulk calcium carbonate structure with M^+ and $\mathrm{BrO_3^-}$ ions from vacuum:

$$\begin{aligned}\Delta E_{\mathrm{exch}} = {} & E\left[\mathrm{Ca}_{n-1}M\left(\mathrm{CO_3}\right)_{n-1}\mathrm{BrO_3}\right]\\ & + \left(E\left[\left(\mathrm{Ca^{2+}}\right)_{\mathrm{gas}}\right] + E\left[\left(\mathrm{CO_3^{2-}}\right)_{\mathrm{gas}}\right]\right)\\ & - E[\mathrm{Ca}_n(\mathrm{CO_3})_n]\\ & + \left(E\left[\left(M^+\right)_{\mathrm{gas}}\right] + E\left[\left(\mathrm{BrO_3^-}\right)_{\mathrm{gas}}\right]\right) \qquad (1)\end{aligned}$$

where $E[\mathrm{Ca}_{n\text{-}1}M(\mathrm{CO_3})_{n\text{-}1}\mathrm{BrO_3}]$ is the energy of the calcium carbonate supercell containing one (M^+ + $\mathrm{BrO_3^-}$) substitution, $E[\mathrm{Ca}_n(\mathrm{CO_3})_n]$ is the energy of the pure calcium carbonate supercell, $E[(M^+)_{\mathrm{gas}}]$ and $E[(\mathrm{BrO_3^-})_{\mathrm{gas}}]$/ $E[(\mathrm{CO_3^{2-}})_{\mathrm{gas}}]$ are the energies of the isolated ions. This analysis allows for comparison between cation substitutions within the same carbonate phase, and comparison of the same cation substitution between carbonate phases. As the exchange energies E_{exch} are calculated with respect to the arbitrary reference of ions in vacuum, the absolute values of these energies carry no physical meaning. The purpose of calculating E_{exch} in this way is to provide a common reference point for comparison of energies between the systems examined. To calculate $\mathrm{Ca^{2+}}$ + $\mathrm{CO_3^{2-}}$ and M^+ + $\mathrm{BrO_3^-}$ as isolated ions in vacuum, within the context our periodic DFT calculations, we obtained the energy of maximally separated ion pairs in supercells of increasing size and extrapolated the result to the limit of an infinitely large cell. Details and plots of the procedure are given in the Supporting Information.

To assess the stability of bromate species in the calcium carbonate phases, we also calculated the solution energies, E_{sol}, which are relative to the thermodynamic competing phase (sodium bromate or potassium bromate):

$$\begin{aligned}\Delta E_{\mathrm{sol}} = {} & E\left[\mathrm{Ca}_{n-1}M(\mathrm{CO_3})_{n-1}\mathrm{BrO_3}\right] - (n-1)E[\mathrm{CaCO_3}]\\ & - E[M\mathrm{BrO_3}] \qquad (2)\end{aligned}$$

where $E[\mathrm{CaCO_3}]$ is the energy per formula unit of the pure calcium carbonate, and $E[M\mathrm{BrO_3}]$ is the energy per formula unit of the competing phase: sodium bromate and potassium bromate. As pure $\mathrm{LiBrO_3}$ is not known, we have excluded lithium from consideration here. The absolute magnitude of the solution energy calculated in this way is more physically meaningful. However, since the ΔE_{sol} energies are not calculated with respect to a common reference, they should not be used for comparison across different polymorphs or compensating cations.

3. RESULTS

For calcite we found 11 inequivalent configurations of one cation/anion pair substitution per supercell, whereas in the aragonite supercell the number of inequivalent

configurations is 48. The energies of each configuration in calcite, after full geometry optimisations, are reported in Table 1. They are given relative to the overall lowest total energy configuration, which is configuration 1 in each case and corresponds to the nearest-neighbour (NN) anion-cation configuration.

In Table 1, d_{min} represents the minimum distance between Br and *M before* relaxation (i.e. between the C and the Ca atoms being substituted in the pure calcite structure). Where the anion-cation distance is the same in more than one case (configurations 4&5 and 9&10), the configurations are still symmetrically inequivalent by virtue of the oxygen atoms, and in these cases, anion-cation distances diverge following structural relaxation.

The binding energies (ε) between the impurities, calculated as the difference between the lowest and highest energies in the configurational spectrum, are shown in Table 2; test calculations with a larger calcite supercell showed that the energy difference between the NN and the most-distant configuration is well converged (within ~ 0.05 eV) at this supercell size. Also in Table 2 are the exchange energies for each host phase and compensating cation, calculated using Eq. (1) under the assumption that the bromate oxyanions and the compensating cations are in relative NN positions.

Table 3 lists the solution energies, calculated using Eq. (2). Solution energies provide thermodynamic insight into formation energy with respect to the competing phase, for example sodium bromate ($NaBrO_3$) or potassium bromate ($KBrO_3$). Here the correct procedure is to evaluate the energy of the mixed system in the absence of NN pairing, because as we will show below, solubility limits (shown as x_m in Table 3) are well below the pairing threshold.

4. DISCUSSION

4.1. Interaction between bromate oxyanions and alkali cations: impurity distributions

There is a clear energy difference between the configuration with nearest-neighbouring impurities and the rest (Table 1), whereas the energy differences between the rest of the configurations are smaller. This is illustrated in Fig. 2, for the case of bromate/lithium substitution in calcite. The NN binding behaviour is also observed for aragonite (data not shown in the table due to the much larger number of configurations, but given in Table S1 of the Supporting Information). The energy distribution across the configurations can be roughly approximated as a sharp drop in energy (the binding energy) at nearest neighbour position, and a constant energy for all the other configurations. Although the energy of configurations beyond the NN pair is not really a constant, the calculated variations among them are significantly less than the difference with respect to the NN configuration, so this simple interaction model captures the NN binding effect but ignores the smaller energy variations at longer distances. The binding energies (ε) between the impurities, given in Table 2, follow the trends Li > Na > K, and aragonite > calcite, which we will attempt to rationalise below.

The simple "binding energy" approximation described above is useful for a discussion of the probability of nearest-neighbour pairing of bromates and compensating cations, based on statistical mechanics. Let us consider a very large supercell of n $CaCO_3$ formula units, where we introduce one cation and one anion substitution, in such a way that the molar fraction of substitution is $x = 1/n$. This supercell can be in one of two states: 1) the binding or pairing state, where the cation and anion substitution form a nearest-neighbour (NN) pair; this state has energy –ε (where ε is the binding energy between the oppositely charged substitutions) and degeneracy zn (where z is the coordination number between NN pairs – there are n sites to substitute the bromate, and for each of those, there are z NN sites to substitute the compensating cations); and 2) the non-binding state, where the cation and anion substitutions are not in NN positions, which has energy zero and degeneracy n^2-zn (i.e. the total number of pair configurations minus the number of NN configurations). Using a Boltzmann's canonical distribution, the probability of NN pairing is then:

$$P_{pair} = \frac{zn \exp\left(\frac{\varepsilon}{k_B T}\right)}{zn \exp\left(\frac{\varepsilon}{k_B T}\right) + n(n-z)} = \frac{1}{1 + \left(\frac{1}{zx} - 1\right) \exp\left(-\frac{\varepsilon}{k_B T}\right)} \quad (3)$$

where k_B is Boltzmann's constant and T is the absolute temperature of equilibration. The above expression is consis-

Table 1
Energies of $M^+ + (BrO_3)^-$ incorporation in calcite (M = Li, Na and K), relative to the configuration with nearest-neighbour (NN) pairing.

Configuration	d_{min} (Br-M^+) (Å)	E_{Li} (eV)	E_{Na} (eV)	E_K (eV)
1 (NN)	3.25	0.00	0.00	0.00
2	4.31	0.60	0.40	0.24
3	6.00	0.51	0.29	0.08
4	6.64	0.57	0.39	0.24
5	6.64	0.43	0.28	0.08
6	7.74	0.63	0.43	0.27
7	7.85	0.56	0.36	0.21
8	9.24	0.59	0.40	0.25
9	9.75	0.59	0.40	0.25
10	9.75	0.59	0.41	0.28
11	10.56	0.63	0.36	0.28

Table 2
Binding energies (ε) between oppositely charged impurity defects, and ion exchange energies (ΔE_{exch}) for calcite and aragonite assuming impurity pairing in nearest-neighbour positions.

Compensating cation	calcite		aragonite	
	ΔE_{exch} (eV)	ε (eV)	ΔE_{exch}	ε (eV)
Li^+	5.59	0.63	5.38	1.08
Na^+	6.42	0.43	6.31	0.65
K^+	7.33	0.28	6.95	0.54

Table 3
Solution energies (ΔE_{sol}) and solubility limits (x_m) for alkali metal-compensated bromate substitution in calcite and aragonite.

	calcite		aragonite	
Competing phase	ΔE_{sol} (eV)	x_m	ΔE_{sol} (eV)	x_m
$NaBrO_3$	1.41	2×10^{-12}	1.71	5×10^{-15}
$KBrO_3$	1.79	1×10^{-15}	1.88	2×10^{-16}

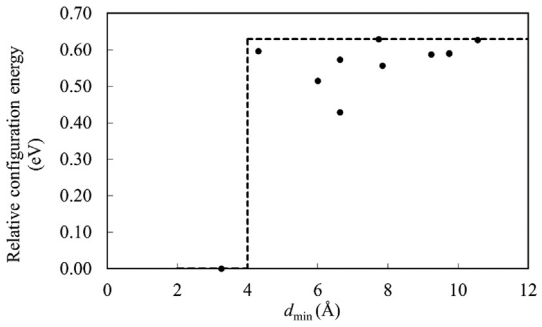

Fig. 2. Plot of relative energy vs minimum distance (d_{min}) between cation impurity and oxyanion impurity in calcite. The dotted line represents the simplified interaction model used for the statistical mechanical analysis: the horizontal dotted line is used to illustrate the pairing energy from this plot (0.63 eV). The vertical dotted line separates the region of NN pairing from the longer distances at which interactions are considered negligible in the simplified interaction model (the precise position of this vertical line is arbitrary).

tent with the equation for energy-dependent site occupancy derived by (Catlow, 1978). In principle it is possible to use a more sophisticated numerical approach, going beyond the minimal supercell to take into account mutual siting of many pairs (Smith et al., 2010), but the more approximate treatment is sufficient here to elucidate the pairing trends. In the limit of strong binding ($\varepsilon \gg k_B T$) and not very low concentration x, the probability of pairing tends to 1, i.e. each substituted cation has a substituted anion in NN position. On the other hand, when the concentration of substitutions is very low, the probability is simply linear on x:

$$P_{pair} \approx zx \exp\left(\frac{\varepsilon}{k_B T}\right). \quad (4)$$

The probabilities of pairing at ambient temperature $T = 300$ K as function of impurity concentration for each phase and compensating cation are shown in Fig. 3. At very low concentrations the probability of pairing increases linearly with x following Eq (4). Above certain threshold concentrations, the pairing probability saturates at 1, which means that all impurity pairs will be found in nearest neighbour configurations. For calcite, these threshold concentrations are $\sim 10^{-11}$ for Li, $\sim 10^{-7}$ for Na, and $\sim 10^{-5}$ for K. For aragonite, the corresponding threshold concentrations for pairing are even lower, following the same trend (Li > Na > K) with the nature of the compensating cation.

Precise bromate concentrations in naturally occurring speleothems are not reported in the literature. The most studied trace element, sulphur, is known to appear in a range of concentrations from roughly 10 to 40 ppm (Frisia et al., 2008) following volcanic activity, though this figure can vary widely depending on the magnitude of volcanic eruption. Marine carbonates have been shown to take up sulphate in the order of 10^3 ppm, two orders of magnitude higher than in speleothem archives (Busenberg and Niel Plummer, 1985). Our analysis above suggests that for concentrations of impurities in the order of several ppm, bromate impurities can be expected to locate in the immediate vicinity of a compensating cation.

4.2. Differences between host phases

The absolute values of the exchange energies reported in Table 2 are irrelevant, with the very high values mainly reflecting the loss of electrostatic stability associated with the aliovalent substitutions, when the isolated ions are taken as reference. But the trends across different cations and host phases are interesting. Compensated bromate incorporation in aragonite is slightly favoured over incorporation in calcite, which is somewhat unexpected given that aragonite is a denser phase than calcite. This contrasts with the behaviour observed for isovalent substitution of carbonates by tetrahedral oxyanions (Midgley et al.,

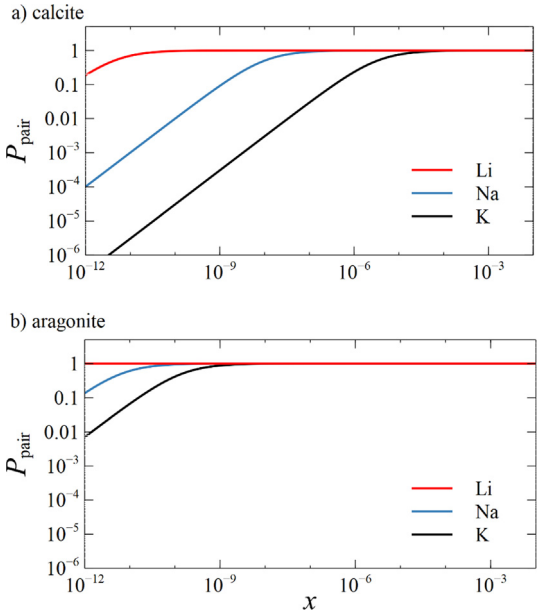

Fig. 3. Pairing probability P_{pair} vs impurity ($M^+ + BrO_3^-$, where M = Li, Na, or K) concentration x at ambient temperature for a) calcite b) aragonite.

2020), where elastic effects, and therefore density, was the primary driver of increased exchange energy.

The stability of the double substitution (anion + cation) is controlled by two factors: 1) a significant favourable electrostatic stabilisation is gained when the distance between the substituting ions is minimised; 2) an unfavourable elastic (lattice) strain energy that comes from distortion of the host crystal, and is particularly important when the distortion is accumulated in a small region of the crystal, i.e. when the ions are in a proximal configuration. Comparing the impurity binding energies of aragonite and calcite with the corresponding exchange energy differences, indicates that the main reason for a lower exchange energy in aragonite is the stronger binding energy between the two impurities. The binding energy is greater in aragonite because the higher phase density affords a shorter anion-cation distance, which is around 2.9 Å in aragonite and 3.2 Å in calcite, prior to structural relaxation. On the other hand, the higher density of aragonite also increases the elastic strain effects, which explains why the exchange energies for aragonite are still similar to those for calcite. The strain effects on the local structures around the impurities are illustrated in Fig. 4 for calcite and in Fig. 5 for aragonite. After relaxation, there is significant ionic reorganisation in aragonite, while in calcite ions occupy the lattice sites of calcium and carbonate without much distortion.

Another trend seen in Table 2 is the increasing substitution energy with increasing cation radius. This may be explained by considering the increased elastic strain imparted on the host crystal when incorporating a larger cation. In the case of K^+ compensation, in addition to the relatively high elastic cost of inserting a large cation, there is a reduction in the binding energy stabilization, due to the combined effect of the distortion fields of both substitutions. It is therefore likely that in geochemical environments, smaller cations are more favourable for charge compensation mechanisms.

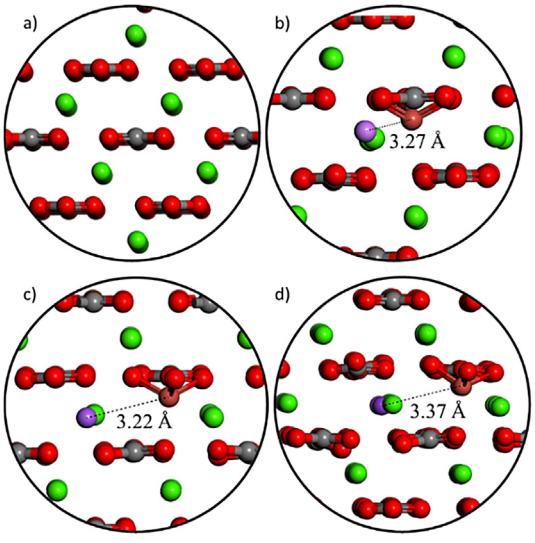

Fig. 4. Optimized local geometries around the double substitution of M^+ and $(BrO_3)^-$ into calcite where a) is pure calcite and the others are bromate-substituted compensated by b) M = Li c) M = Na d) M = K.

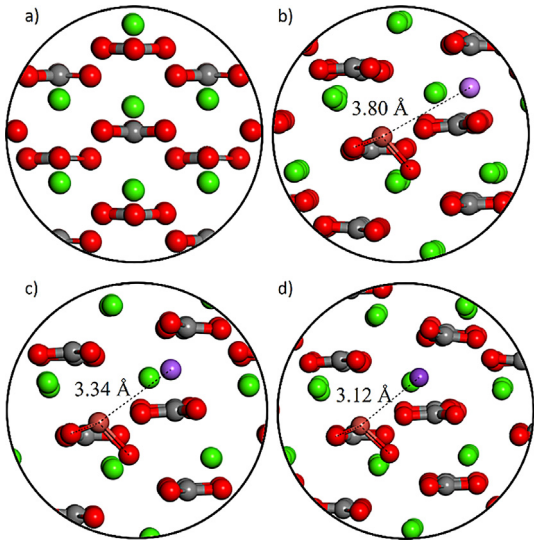

Fig. 5. Optimized local geometries around the double substitution of M^+ and $(BrO_3)^-$ into aragonite where a) is pure aragonite and the others are bromate-substituted compensated by b) M = Li c) M = Na d) M = K.

4.3. Stability of substitutions against competing phases

We now discuss the calculated solution energies, presented in Table 3. Whether a certain level of trace impurity incorporation is stable or not with respect to separation into a competing phase depends on the balance between the enthalpy of mixing

$$\Delta H_{\mathrm{mix}} \approx x\Delta E_{\mathrm{sol}} \tag{5}$$

and the configurational entropy effect:

$$-TS_{\mathrm{conf}} = 2k_{\mathrm{B}}T[x\ln x + (1-x)\ln(1-x)] \tag{6}$$

that stabilises the mixing. The factor of 2 in Eq. (6) appears because there are two independently disordered species with concentration x (when the concentration is well below the pairing threshold). As in previous work (Grau-Crespo et al., 2011; Midgley et al., 2020) the solubility limit or maximum concentration of impurity thermodynamically stable against phase separation can therefore be estimated from the solution energy:

$$x_{\mathrm{m}} \approx \exp\left(-\frac{\Delta E_{\mathrm{sol}}}{2k_{\mathrm{B}}T}\right) \tag{7}$$

For Na-compensated bromate substitution in calcite, this value is $\sim 2 \times 10^{-12}$, and for the same substitution in aragonite is $\sim 5 \times 10^{-15}$. The values for K-compensated substitutions are even lower (see Table 3). The low values suggest that bromate substitution at ppm level and even at ppb level in bulk lattice sites is metastable with respect to phase separation, at least when compensated by Na or K. This conclusion should be accompanied by some caveats. First, the solubility limits via other charge compensating schemes (e.g. with Li^+, or even H^+ which has

not been considered here) might be much higher, leading to thermodynamically stable bromate substitution. Second, metastable bulk incorporation can still occur due to the complicated kinetics of mineral growth. For example, it is known that sulphate can partially incorporate in the bulk of calcite, even if the calculated solubility limits obtained for sulphate (Midgley et al., 2020) are very low (in fact much lower than the solubility limits obtained here for bromate). The higher solution limit of bromate compared to sulphate and molybdate is mainly due to the lower strain around the oxyanion impurity when the fourth, apical oxygen is not present, even if the trigonal pyramidal bromate ion is not a perfect fit to substitute the trigonal planar carbonate anion.

4.4. Geochemical implications

Several physical chemical and biological processes can influence trace element concentrations in speleothems as trace element composition of cave drip water is influenced by the atmosphere, soil, aquifer and cave environment. Though the fluid- dominated trace element variations are fairly well known for the most frequently used trace elements (*e.g.*, Mg, Sr, P, U, P), the effect of other factors and mechanisms controlling trace element incorporation into speleothem carbonate phases remains poorly understood. This is particularly true for bromine, which, as discussed in the Introduction, can be used to detect volcanic eruptions in speleothems. To date, it remains unclear how bromine incorporates into speleothem carbonate phases, and which factors control the extent of its incorporation. Our study offers a first theoretical approximation to the problem and some initial insights of geochemical interest.

An important question is to what extent the Br content in the drip water is proportionally reflected in the Br content of the carbonate minerals. The (imperfect) equilibrium between the solid and the fluid can be described by a partitioning coefficient $D = (n_{Br}^{solid}/n_{C}^{solid})/(n_{Br}^{fluid}/n_{C}^{fluid})$, where the n values refer to the molar concentrations in the solid or fluid. Our hypothesis here is that bromine incorporates in the form of lattice bromate oxyanions via the aliovalent substitution of carbonate oxyanions. Contrasting with the case of isovalent substitutions, where the partition coefficient is mainly affected by the size and shape differences between the incorporated and the replaced ions and is approximately constant at a given temperature, the extent of aliovalent substitutions is affected by the charge imbalance and the mechanisms of its compensation. In this case, the nature and concentration of compensating ions in the fluid will affect D, even if the interaction between the oppositely charged impurities is weak. This effect has been investigated, for example, for rare earth elements (REE^{3+}) incorporation in calcite, compensating by concurrent incorporation of Na^{+} compensating cations (Voigt et al., 2017); in this case the uptake of REE in calcite depends on the concentration of Na^{+} in the fluid.

In the case of bromine incorporation in speleothems, the partition coefficient D will depend on the concentration of alkali cations in the drip water and the thin water film in near equilibrium with the carbonate minerals. Although not considered in this study, compensating with protons might also be possible, which will make the partition coefficient for bromine strongly pH dependent. Given that the bromate impurities and the compensating cations are predicted to be in close interaction and proximity within the crystal structure, the effect of the nature and concentration of compensating cations on the bromine partition coefficient will be even stronger. This analysis suggests that increases in the fluid's Br content might not reflect proportionally on the Br content in the solid, even under the assumption of equilibrium, and that the behaviour would depend on the overall chemical composition of the aqueous solution. Minor changes in Br content of the fluid, for example from small or remote volcanic eruptions, might then escape detection by the speleothem method. Due to the different behaviour of calcite and aragonite in the incorporation of bromate and compensating ions, the phase composition of the speleothems will also have a strong effect on the Br trace concentration in the speleothems.

Our results point at the need for further experimental investigation of the complex phenomenon of bromate incorporation. It would be useful, for example, if characterization techniques like Extended X-ray Adsorption Fine Structure (EXAFS) could be used to probe the local structure around the bromine species in carbonate minerals, not only to confirm the substitution of bromine as bromate species (as has been done by Podder et al. (2017) to corroborate the substitution of iodine as iodate species), but also to investigate the presence of compensating cations in the second coordination sphere. Such information is essential to create quantitative models of Br incorporation in carbonate minerals, that would then allow a more robust interpretation of speleothem records of volcanic eruptions.

5. CONCLUSIONS

We have presented a computer simulation study of the incorporate of bromate ions as aliovalent substitutional impurities in the anion sites of calcium carbonate minerals calcite and aragonite. The chemistry associated to the incorporation of these species is more sophisticated than that of isovalent substitutions of carbonate by sulphate or molybdate, that we investigated previously (Midgley et al., 2020; Midgley et al., 2021) due to the additional complexity associated to the possible charge compensating schemes, and the interaction of bromate impurities with the charge-compensating cations. Our calculations provide a prediction of the pairing thresholds, i.e. the concentrations above which the binding energy between oppositely charged impurities at nearest-neighbour positions dominate over the entropic tendency to disassociate the impurities. We have demonstrated that the pairing is slightly stronger in aragonite than in calcite, and that it decreases down the group of alkali metals as compensating cations (Li > Na > K). Assuming thermodynamic equilibrium, it can be expected that bromate substitution at ppm-level occurs with a very high degree of pairing of the bromate ion with the compensating cations in nearest-neighbour positions in the lattice.

Based on our simulations, we expect cations of smaller radii to preferentially incorporate into the carbonate struc-

ture as they cause lower degrees of lattice strain on the host. Where there is low concentration of sodium or lithium in the local aqueous environment, bromate is unlikely to be stabilised in the carbonate phase, therefore counterion abundance may be an important consideration when interpreting bromine-containing trace-element records. An important scenario for future investigation is charge compensation by protons, which leads to interesting chemistry as the thermodynamics becomes pH dependent. The solution energy calculations indicate that bromate substitution compensated by sodium or potassium cations is metastable with respect to phase separation of the impurities as solid $NaBrO_3$ or $KBrO_3$ phases, respectively. However, the solubility limits of bromate in calcite and aragonite are still higher than those calculated for sulphate or molybdate, so the thermodynamic driving force for bromate to separate into a competing phase is relatively weaker. This analysis suggests more bulk substitution of bromate in calcite and aragonite, compared to sulphate and molybdate.

Our findings provide structural and atomic-level insight that may help the interpretation of bromine records in speleothems. Our work highlights that bromine abundance is expected to be carbonate phase specific, *i.e.* relative abundances of calcite and aragonite are important considerations. Also, the abundance of possible compensating cations in solution will have an important effect on the final amount of bromine incorporated. Monovalent ions should be detected proximal to bromine impurities, where there is a strong thermodynamic preference for smaller ions. Abundance of lithium in the bromine-containing speleothem is likely to be representative of the amount of lithium in the local aqueous environment around the time of speleothem formation, which may significantly skew the detected levels of bromine compared with the deduced volcanic eruption magnitude. These are all key considerations when interpreting speleothem archive data.

6. DATA AVAILABILITY

All the data related to this work (input and output files of the computer simulations) are available online at the Zenodo repository https://doi.org/10.5281/zenodo.5035293.

Declaration of Competing Interest

The authors declare that they have no known competing financial interests or personal relationships that could have appeared to influence the work reported in this paper.

ACKNOWLEDGEMENTS

S. D. Midgley acknowledges funding for his PhD studentship from the Natural Environment Research Council through the SCENARIO DTP (grant ref NE/L002566/1). This work made use of ARCHER, the UK's national high-performance computing service, via the UK's HPC Materials Chemistry Consortium, which is funded by EPSRC (EP/R029431), and of the Young supercomputer, via the UK's Materials and Molecular Modelling Hub, which is partially funded by EPSRC (EP/T022213/1).

APPENDIX A. SUPPLEMENTARY MATERIAL

A Supporting Information file contains details of the calculation of energies of ions in vacuum, and the energy data for all substitution configurations in aragonite.

Supplementary data to this article can be found online at https://doi.org/10.1016/j.gca.2022.02.028.

REFERENCES

Badertscher S., Borsato A., Frisia S., Cheng H., Edwards R. L., Tüysüz O. and Fleitmann D. (2014) Speleothems as sensitive recorders of volcanic eruptions – the Bronze Age Minoan eruption recorded in a stalagmite from Turkey. *Earth Planet. Sci. Lett.* **392**, 58–66.

Blöchl P. E. (1994) Projector augmented-wave method. *Phys. Rev. B* **50**, 17953–17979.

Bobrowski N., Hönninger G., Galle B. and Platt U. (2003) Detection of bromine monoxide in a volcanic plume. *Nature* **423**, 273–276.

Busenberg E. and Niel Plummer L. (1985) Kinetic and thermodynamic factors controlling the distribution of SO_3^{2-} and Na^+ in calcites and selected aragonites. *Geochim. Cosmochim. Acta* **49**, 713–725.

Catlow C. (1978) Ion distribution functions for complex solids and their application to the conductivity of glasses. *Phys. Status Solidi A* **46**, 191–198.

De Choudens-Sanchez V. and Gonzalez L. A. (2009) Calcite and aragonite precipitation under controlled instantaneous supersaturation: Elucidating the role of $CaCO_3$ saturation state and Mg/Ca ratio on calcium carbonate polymorphism. *J. Sediment. Res.* **79**, 363–376.

De Villiers J. P. R. (1971) Crystal structures of aragonite, strontianite, and witherite. *Am. Mineral.* **56**(5–6), 758–767.

Dorale J. A., Edwards R. L., Calvin-Alexander, Jr, E., Shen C. C., Richards D. A. and Cheng H. (2004) *Studies of Cave Sediments*. Springer, US, Boston, MA.

Engel A. O. and Perlmutter-Hayman B. (1953) The decomposition of hypobromite and bromite solutions. *J. Am. Chem. Soc.* **76**, 2010–2015.

Fairchild I. J. and Treble P. C. (2009) Trace elements in speleothems as recorders of environmental change. *Quat. Sci. Rev.* **28**, 449–468.

Feng X. and Redfern S. A. T. (2018) Iodate in calcite, aragonite and vaterite $CaCO_3$: Insights from first-principles calculations and implications for the I/Ca geochemical proxy. *Geochim. Cosmochim. Acta* **236**, 351–360.

Finch A. A., Shaw P. A., Weedon G. P. and Holmgren K. (2001) Trace element variation in speleothem aragonite: potential for palaeoenvironmental reconstruction. *Earth Planet. Sci. Lett.* **186**, 255–267.

Friedrich W. L., Kromer B., Friedrich M., Heinemeier J., Pfeiffer T. and Talamo S. (2006) Santorini eruption radiocarbon dated to 1627–1600 BC. *Science* **312**, 548.

Frisia S., Borsato A. and Susini J. (2008) Synchrotron radiation applications to past volcanism archived in speleothems: An overview. *J. Volcanol. Geoth. Res.* **177**, 96–100.

Given R. K. and Wilkinson B. H. (1985) Kinetic control of morphology, composition, and mineralogy of abiotic sedimentary carbonates. *J. Sediment. Res.* **55**, 109–119.

González-López J., Ruiz-Hernández S. E., Fernández-González Á., Jiménez A., de Leeuw N. H. and Grau-Crespo R. (2014) Cobalt incorporation in calcite: Thermochemistry of (Ca, Co) C_O3 solid solutions from density functional theory simulations. *Geochim. Cosmochim. Acta* **142**, 205–216.

Grau-Crespo R., de Leeuw N. H., Hamad S. and Waghmare U. V. (2011) Phase separation and surface segregation in ceria–zirconia solid solutions. *Proc. Roy. Soc. A - Math. Phys.* **467**, 1925–1938.

Grau-Crespo R., Hamad S., Catlow C. R. A. and Leeuw N. H. D. (2007) Symmetry-adapted configurational modelling of fractional site occupancy in solids. *J. Phys. - Condens. Mat.* **19**, 256201.

Hartland A., Fairchild I. J., Lead J. R., Borsato A., Baker A., Frisia S. and Baalousha M. (2012) From soil to cave: Transport of trace metals by natural organic matter in karst dripwaters. *Chem. Geol.* **304–305**, 68–82.

Hörmann C., Sihler H., Bobrowski N., Beirle S., Penning de Vries M., Platt U. and Wagner T. (2013) Systematic investigation of bromine monoxide in volcanic plumes from space by using the GOME-2 instrument. *Atmos. Chem. Phys.* **13**, 4749–4781.

Kerisit S. N., Smith F. N., Saslow S. A., Hoover M. E., Lawter A. R. and Qafoku N. P. (2018) Incorporation modes of iodate in calcite. *Environ. Sci. Technol.* **52**, 5902–5910.

Kresse G. and Furthmüller J. (1996a) Efficiency of ab-initio total energy calculations for metals and semiconductors using a plane-wave basis set. *Comput. Mater. Sci.* **6**, 15–50.

Kresse G. and Furthmüller J. (1996b) Efficient iterative schemes for ab initio total-energy calculations using a plane-wave basis set. *Phys. Rev. B* **54**, 11169–11186.

Kresse G. and Joubert D. (1999) From ultrasoft pseudopotentials to the projector augmented-wave method. *Phys. Rev. B* **59**, 1758–1775.

Lee C. L. and Lister M. W. (1971) The decomposition of aqueous sodium bromite. *Can. J. Chem.* **49**, 2822–2826.

Markgraf S. and Reeder R. (1985) High-temperature structure refinements of calcite and magnesite. *Am. Mineral.* **70**, 590–600.

Marshall D., Ghaleb B., Countess R. and Gabities J. (2009) Preliminary paleoclimate reconstruction based on a 12,500 year old speleothem from Vancouver Island, Canada: stable isotopes and U-Th disequilibrium dating. *Quat. Sci. Rev.* **28**, 2507–2513.

McCarroll D. and Loader N. J. (2004) Stable isotopes in tree rings. *Quat. Sci. Rev.* **23**, 771–801.

Midgley S. D., Di Tommaso D., Fleitmann D. and Grau-Crespo R. (2021) Sulfate and molybdate incorporation at the calcite–water interface: insights from ab initio molecular dynamics. *ACS Earth Space Chem.* **5**, 2066–2073.

Midgley S. D., Taylor J. O., Fleitmann D. and Grau-Crespo R. (2020) Molybdenum and sulphur incorporation as oxyanion substitutional impurities in calcium carbonate minerals: a computational investigation. *Chem. Geol.* **553** 119796.

Minnis P., Harrison E. F., Stowe L. L., Gibson G. G., Denn F. M., Doelling D. R. and Smith W. L. (1993) Radiative climate forcing by the mount Pinatubo Eruption. *Science* **259**, 1411.

Perdew J. P., Burke K. and Ernzerhof M. (1996) Generalized gradient approximation made simple. *Phys. Rev. Lett.* **77**, 3865.

Podder J., Lin J., Sun W., Botis S., Tse J., Chen N., Hu Y., Li D., Seaman J. and Pan Y. (2017) Iodate in calcite and vaterite: Insights from synchrotron X-ray absorption spectroscopy and first-principles calculations. *Geochim. Cosmochim. Acta* **198**, 218–228.

Railsback L. B., Brook G. A., Chen J., Kalin R. and Fleisher C. J. (1994) Environmental controls on the petrology of a late Holocene speleothem from Botswana with annual layers of aragonite and calcite. *J. Sediment. Res.* **64A**, 147–155.

Robock A. (2000) Volcanic eruptions and climate. *Rev. Geophys.* **38**, 191–219.

Robock A. and Free M. P. (1995) Ice cores as an index of global volcanism from 1850 to the present. *J. Geophys. Res. - Atmos.* **100**, 11549–11567.

Ruiz-Hernandez S. E., Grau-Crespo R., Ruiz-Salvador A. R. and De Leeuw N. H. (2010) Thermochemistry of strontium incorporation in aragonite from atomistic simulations. *Geochim. Cosmochim. Acta* **74**, 1320–1328.

Severi M., Udisti R., Becagli S., Stenni B. and Traversi R. (2012) Volcanic synchronisation of the EPICA-DC and TALDICE ice cores for the last 42 kyr BP. *Clim. Past* **8**, 509–517.

Sigl M., McConnell J. R., Layman L., Maselli O., McGwire K., Pasteris D., Dahl-Jensen D., Steffensen J. P., Vinther B. and Edwards R. (2013) A new bipolar ice core record of volcanism from WAIS Divide and NEEM and implications for climate forcing of the last 2000 years. *J. Geophys. Res. - Atmos.* **118**, 1151–1169.

Smith K. C., Fisher T. S., Waghmare U. V. and Grau-Crespo R. (2010) Dopant-vacancy binding effects in Li-doped magnesium hydride. *Phys. Rev. B* **82,** 134109.

St Pierre E., Zhao J. and Reed E. (2009) Expanding the utility of Uranium-series dating of speleothems for archaeological and palaeontological applications. *J. Archaeol. Sci.* **36**, 1416–1423.

Theys N., Van Roozendael M., Dils B., Hendrick F., Hao N. and De Mazière M. (2009) First satellite detection of volcanic bromine monoxide emission after the Kasatochi eruption. *Geophys. Res. Lett.* **36,** L03809.

Ünal-İmer E., Shulmeister J., Zhao J.-X., Tonguç Uysal I., Feng Y.-X., Duc Nguyen A. and Yüce G. (2015) An 80 kyr-long continuous speleothem record from Dim Cave, SW Turkey with paleoclimatic implications for the Eastern Mediterranean. *Sci. Rep.* **5**, 13560.

Voelker A. H. L. (2002) Global distribution of centennial-scale records for Marine Isotope Stage (MIS) 3: a database. *Quat. Sci. Rev.* **21**, 1185–1212.

Voigt M., Mavromatis V. and Oelkers E. H. (2017) The experimental determination of REE partition coefficients in the water-calcite system. *Chem. Geol.* **462**, 30–43.

Wang Q., Grau-Crespo R. and de Leeuw N. H. (2011) Mixing thermodynamics of the calcite-structured (Mn, Ca)C_O3 solid solution: A computer simulation study. *J. Phys. Chem. B* **115**, 13854–13861.

Yalcin K., Wake C. P., Kreutz K. J., Germani M. S. and Whitlow S. I. (2007) Ice core paleovolcanic records from the St. Elias Mountains, Yukon, Canada. *J. Geophys. Res.* **112**, D08102.

Zielinski G. A. (2000) Use of paleo-records in determining variability within the volcanism–climate system. *Quat. Sci. Rev.* **19**, 417–438.

Zielinski G. A., Mayewski P. A., Meeker L. D., Whitlow S., Twickler M. S., Morrison M., Meese D. A., Gow A. J. and Alley R. B. (1994) Record of volcanism since 7000 B.C. from the GISP2 Greenland ice core and implications for the volcano-climate system. *Science* **264**, 948–952.

Associate editors: Mariette Wolthers and Jeffrey G. Catalano